Thermochimica Acta 498 (2010) 81–91

Contents lists available at ScienceDirect

Thermochimica Acta

journal homepage: www.elsevier.com/locate/tca

Matrix assisted pulsed laser evaporation of zinc benzoate for ZnO thin films and non-isothermal decomposition kinetics

A. Rotaru[a,*], C. Constantinescu[a], Anca Mândruleanu[b], P. Rotaru[c], A. Moldovan[a], Katarina Győryová[d], Maria Dinescu[a], V. Balek[e]

[a] INFLPR – National Institute for Laser, Plasma and Radiation Physics, PPAM – Lasers Department, 409 Atomiştilor Bvd., Măgurele, RO-077125, Bucharest, Romania
[b] ASE – Academy of Economic Studies, FABIZ, 5-7 M. Moxa Str., RO-010961, Bucharest, Romania
[c] University of Craiova, Faculty of Physics, 13 A.I. Cuza Str., Craiova, RO-200585, Dolj, Romania
[d] P.J. Šafarik University, Faculty of Science, Department of Inorganic Chemistry, 11 Moyzesova Str., Košice, Slovakia
[e] Nuclear Research Institute, Central Analytic Laboratory, CZ 25068, Řez, Czech Republic

ARTICLE INFO

Article history:
Received 5 July 2009
Received in revised form 3 October 2009
Accepted 6 October 2009
Available online 13 October 2009

Keywords:
Zinc benzoate
Thin films
MAPLE
Thermal analysis
Non-isothermal kinetics
ZnO

ABSTRACT

Zinc(II) coordination compounds may provide a better source for ZnO thin films obtaining, since ZnO was found as the final product of their thermal decomposition. Thin films of zinc benzoate have been obtained on silicon substrates by matrix assisted pulsed laser evaporation (MAPLE) technique, using a Nd:YAG laser working at 266 nm. A comparative study of 1% zinc benzoate frozen solution in methanol at different fulences was carried out for 20,000 laser pulses; for the best deposition fluence a double deposition time was employed. Comparative thermal analysis and non-isothermal kinetic investigation of $Zn(C_6H_5COO)_2{\cdot}2H_2O$ dehydration and decomposition was performed. Thin films of ZnO have been obtained by thermal treatment of the MAPLE obtained thin films, according to the thermal analysis and decomposition kinetics of zinc benzoate. The obtained morphologies, before and after thermal treatment, have been investigated by atomic force microscopy (AFM).

1. Introduction

Zn(II) coordination compounds have proven to be active as antibacterial materials and similar benzoate-based compounds have widely been used as pharmaceuticals [1–9]. The ease of obtaining such coordination compounds and the high thermal stability of some of them (*i.e.* $Zn(C_6H_5COO)_2$ initial decomposition temperature >180°C [10,11]) enables employing as thin films for biological purposes. Since ZnO was found to be the final product of the thermal decomposition of many Zn-based complex compounds, these may be used as precursors for reduced-scale materials synthesis [12–14]. Zinc acetate, zinc salicylate, zinc benzoate, zinc butyrate and their crystallization products with ligands such as urea, caffeine, thiourea, may be also a better source for ZnO thin films processing [15–18].

Thin films may be obtained by various deposition methods, but the laser assisted techniques produce the smoothest and continuous surfaces – the main, most popular and important technique is pulsed laser deposition (PLD). Unfortunately, PLD may be usually used as a deposition method for simple compounds only [19,20] (when for ZnO, only using the basic oxide target [21–23] or Zn target in oxygen atmosphere [24–26]). When the laser beam interacts with the target, the material is ablated and becomes plasma, some elements recombining in the form of basic inorganic compounds while the organic parts pyrolyze. This is not only due to the relatively high laser energy fluences, that induce photothermal decompositions, but also to the impossibility of transferring more complicated structural fragments. The main advantage of laser-assisted deposition techniques is the perpendicular manner the material plume reaches the surface of the substrate and by tilting the late, inaccessible areas may be covered. Anglos and coworkers [27,28] used random laser action on inorganic and organic nanocomposites in order to transform the particulate grain structure of the ZnO thin film into a porous channel-like network. In order to eliminate the difficulties, a new deposition technique – matrix assisted pulsed laser evaporation (MAPLE), also based on laser-matter interaction type, was developed [29–31].

In this paper we report on the use of MAPLE technique for the deposition of thin films of zinc benzoate. The films were then thermally treated in order to obtain layers of ZnO according to the thermal analysis and decomposition kinetics of the complex precursor. Thermal analysis of $Zn(C_6H_5COO)_2{\cdot}2H_2O$ powder was carried out in both air flow and argon flow for a better understanding of its thermal behavior regardless the employed

* Corresponding author. Tel.: +40 745379205.
E-mail address: andrei.rotaru@inflpr.ro (A. Rotaru).

0040-6031/$ – see front matter © 2009 Elsevier B.V. All rights reserved.
doi:10.1016/j.tca.2009.10.006

gaseous atmosphere. Kinetic investigation of $Zn(C_6H_5COO)_2{\cdot}2H_2O$ non-isothermal decomposition may provide precious information on the complexity of the processes that happen during ZnO formation. A literature survey indicated such complex thermal and kinetic behaviours for several Zn(II) coordination compounds [32–38]

2. Overview on thin films and methodological features of MAPLE technique

The debate "thin *vs.* thick film" applications, manufacture techniques, quality and production costs is well-known; regardless of their use (renewable energy collectors, solar cells, gas sensors, semiconducting, protective coatings or biocompatible layers), both are precious devices for our era. In Mark J. Madou's book "Fundamentals of microfabrication. The science of miniaturization" [39], a comparison between thin and thick film sensor technologies is carried out. The discussion is being focused mainly on the economic and technical aspects [40]. The high initial investments and >$400k for production lines costs, balanced by versatile characteristics (small dimensions, reproducibility, in *vivo* use, etc.) and their significant applications, have increased thin films mass production sales on industrial and medical markets up to 10 times when comparing to the thick films sales, finally stimulating cheaper selling prices.

Not only small dimension thin films are valuable, but also the large area ones [41]; for example, the intelligent use of free of charge and unlimited solar energy [42] requires photovoltaic (PV) cells which contain as indispensable part large area capture layers. Aquaviva et al. [41] designed and built a pulsed laser deposition system that allows three-dimensional depositions on hundreds of cm^2. Wise placement of solar cells on houses' roofs in hot zones, and on the other side noise- and pollution-free, minimal maintenance and long service lifetimes [42] have doubled their efficiency from 6% to 12% only in the last 5 years and forecast for PV market an accelerating increase.

Such an example would be ZnO, which is not only an II–IV wide-bandgap semiconductor (bandgap energy of 3.3 eV) [43], but when prepared with high electronic conductivity, may be used also in the solar cells. This can be easily acquired for n-type materials, but has a lack of reproducibility for the p-type ones [43]. Various deposition methods may be used, but Sputtering and metal-organic chemical vapor deposition (MOCVD) are preferred when large area covering is needed. However, MOCVD is limited by the vaporization condition the precursors should accomplish. On the other side, MAPLE technique should solve this difficulty and moreover, it can replace the temperature program for controlling the molecules release, by adjusting the laser fluence.

MAPLE technique is similar to the PLD technique; the only difference consists in diluting the material in a volatile non-interacting solvent further to be frozen or mixing it with another solid which represents this time the matrix. By irradiating the prepared target with a pulsed laser beam, only the solvent/matrix absorbs the laser wavelength and thus the system is evaporated. The solute material is collected on a substrate placed in front the target, while the solvent is pumped out or the solid matrix is pyrolyzed or burnt. When applying MAPLE technique, one must be confident that the compound does not absorb the selected laser radiation. Therefore, in the case of molecular compounds deposition by MAPLE, only the molecules of the appropriate material are collected on the substrate. Such a non-destructive technique accurately solves the deposition problem of complex chemical structures (organic and bioorganic molecules, coordination compounds, polymers, *etc.*) [19,20,29–31,44–51]. MAPLE technique provides a gentle mechanism of transferring small and large molecular weight species or compounds possessing weak bonds (coordination complexes) from a condensed phase into the vapor phase.

Zhigilei and co-workers carried out parametric investigations, both experimental and simulated MAPLE depositions [52–57]. They have simulated the mechanism of laser ablation and molecular dynamics [52–54] in MAPLE depositions and also experimentally investigated them in a group of papers [55–57]. A surface clustering mechanism of a polymer–matrix system was proposed, with the solvent escaping the film while the polymer inflates [55] – rearrangement of the thin film after deposition.

A great advantage of MAPLE technique over PLD is the versatile tailoring of nanostructures; while for PLD depositions of ZnO only masks may be used for creating punctual structures, the MAPLE deposited Zn(II) complexes may be locally thermal decomposed more wisely to ZnO by using a lower frequency laser beam, the remained surrounding Zn(II) complex to be further washed out with solvent.

3. Experimental

$Zn(C_6H_5COO)_2{\cdot}2H_2O$ was prepared by reacting $ZnCO_3$ with benzoic acid (Aldrich) in aqueous medium, under continuous stirring in hot water at 70 °C, followed by crystallization in water bath and filtering, as described in [11]. Previously, solid $Zn(OH)_2$ was obtained from $ZnCl_2$ and Na_2CO_3, by removing NaCl with water.

Thin films of zinc benzoate were obtained on silicon substrates by MAPLE technique, using a "Surelite II" Nd:YAG laser from Continuum Company, working at 266 nm and a repetition rate of 10 Hz. The targets were prepared by freezing the solution of coordination compound in methanol (melting temperature: −97 °C) using liquid nitrogen, while continuous monitoring the target's temperature and maintaining it refrigerated between −115 °C and −110 °C in the deposition chamber. The target holder was rotated with a motion feedthrough of 20 rotations/min, driven by a motor, while the laser beam describing a circular movement onto the sample and every 5 min changing its position in order to avoid gaps' formation in the target. The Si(1 0 0) collecting substrates, of about 1 cm^2 each, have been placed 4 cm far from the target, in a parallel position to the first. Usually, the solution must be of 0.1–2.0% because of the hard laser interaction with the solid target; here, a comparative study of 1% frozen solutions in methanol at different fulences (from 0.1 to 1.3 $J\,cm^{-2}$) and 20,000 laser pulses was carried out. For the best depositions (0.5 and 0.7 $J\,cm^{-2}$), double timing experiments (40,000 laser pulses) were further carried out. The deposition experiments were performed in vacuum, for pressures varying between 8×10^{-3} and 9×10^{-3} $N\,m^{-2}$ (obtained with a turbomolecular Pfeiffer-Balzers TPU 170 pump: 170 $L\,s^{-1}$), using air as background gas.

The preservation of zinc benzoate molecules after the laser beam interaction with the frozen target and the obtaining of the thin films were investigated by Fourier transformed infrared spectroscopy, using a Jasco FTIR-6300 type A spectrometer, in the range 400-7800 cm^{-1}.

Thermal analysis (TG, DTG, DTA and DSC) measurements of $Zn(C_6H_5COO)_2{\cdot}2H_2O$ crystal powder have been carried out in both air flow and argon flow (150 mL min^{-1}), under non-isothermal linear regimes. A horizontal "Diamond Differential/Thermogravimetric" Analyzer from PerkinElmer Instruments was used during the experiments, having as reference inert α-Al_2O_3 powder. Samples from 1 to 2 mg, contained in α-Al_2O_3 crucibles, were heated from room temperature to 1000 °C, with the programmed heating rates of: 2, 6 and 10 K min^{-1}. Real heating rates in the samples were found to be: 2.08, 6.30, 10.54 K min^{-1} (air flow) and 2.02, 6.12, 10.22 K min^{-1} (argon flow). The thermal treatment of MAPLE deposited thin films of zinc coordination compound

Table 1
Experimental MAPLE deposition parameters and thin films morphology (40 μm × 40 μm) results by AFM.

Laser fluence (J cm^{-2})	Laser pulses	R_{P-V} (peak to valley) (nm)	R_Q (roughness) (nm)	Observations
0.1	20,000	–	–	No deposition
0.3	20,000	772	101	Disparate droplets deposition
0.4	20,000	283	44	Disparate droplets deposition
0.5	20,000	268	13	Several circular areas of deposition
0.5	40,000	471	44	Uniform circular area deposition
0.7	20,000	927	132	Uniform circular area deposition
0.7	40,000	660	97	Uniform circular area deposition
1.0	20,000	807	129	High amount of material and irregular deposition
1.3	20,000	1187	202	High amount of material and irregular deposition; burned aspect of the thin film

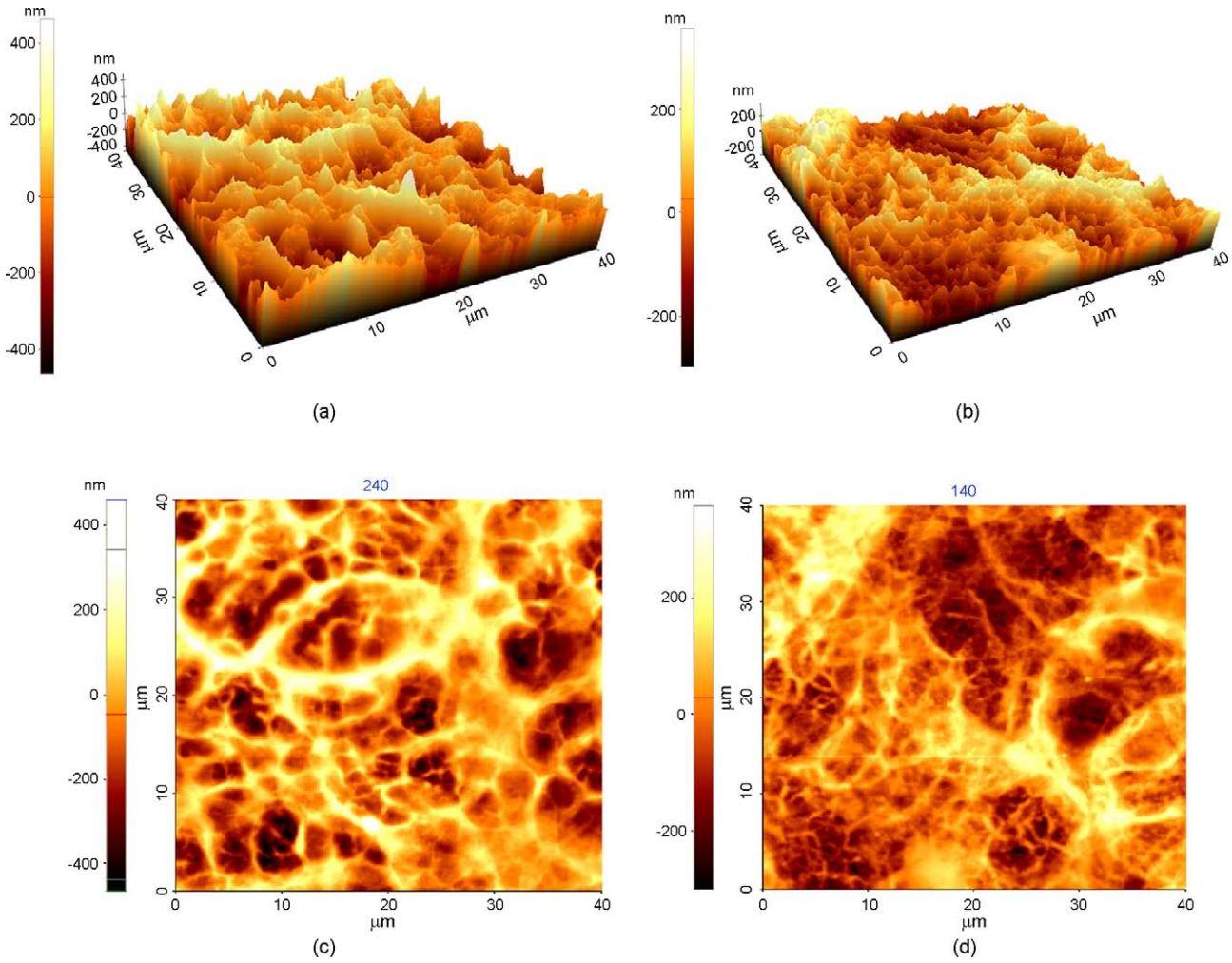

Fig. 1. 3D AFM images of zinc benzoate thin films by MAPLE, obtained at 0.7 J cm^{-2} laser fluence for (a) 20,000 pulses; (b) 40,000 pulses and 2D AFM images of zinc benzoate thin films by MAPLE, obtained at 0.7 J cm^{-2} laser fluence for (c) 20,000 pulses; (d) 40,000 pulses.

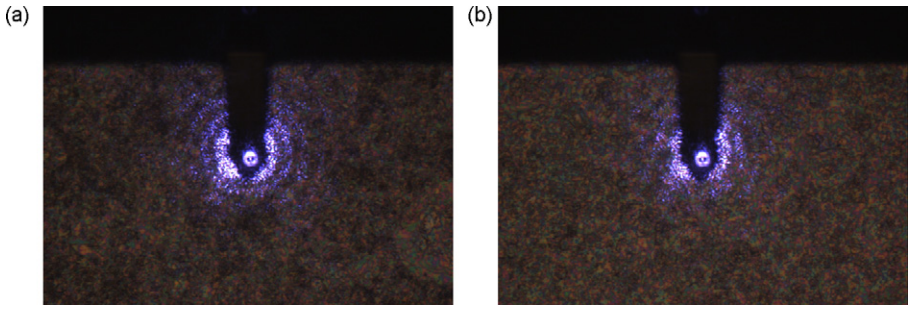

Fig. 2. Optical microscopy images of zinc benzoate thin films by MAPLE, obtained at 0.7 J cm^{-2} laser fluence, for (a) 20,000 pulses; (b) 40,000 pulses.

on Si substrates was performed in static air atmosphere using a Nabertherm L3/11/B170 muffle furnace (Nabertherm Company, Germany), from room temperature to 600 °C, with increasing temperature by 1 K min^{-1}, according to the thermal analysis and kinetic studies results. The samples have been carefully cooled at the same rate in order to avoid substrates' cracking.

Thin films morphology, before and after the thermal treatment, was investigated by atomic force microscopy (AFM) using a "Park XE-100" instrument from Park Systems, in non-contact mode.

4. Results and discussion

4.1. Zinc benzoate thin films by MAPLE technique

Thin films of zinc benzoate have been obtained on Si substrates by MAPLE technique, following the procedure described in the Section 2. First, the experiments were carried out for a duration of 33 min (20,000 laser pulses). For low laser fluences (*e.g.* 0.1 J cm^{-2}) there is no deposition to be found on the substrates, while when increasing laser fluence (Table 1, until 0.5 J cm^{-2}) the Si substrates are not entirely covered, but the peak to valley (R_{P-V}) and roughness (R_Q) values continuously decrease. The ablated and thus deposited material increases with increasing fluence (from 0.7 to 1.3 J cm^{-2}), therefore thin films' smoothness and continuity decreases (Table 1).

The laser fluence of 1.0 J cm^{-2} proved to transfer more material, but when analyzing the obtained thin film, it revealed worse morphology compared to the sample at 0.7 J cm^{-2}. When selecting the laser fluence of 1.3 J cm^{-2}, the obtained films looked as already burned and with increased roughness and peak to valley values (Table 1), therefore it seems to be much too high.

For a double deposition duration (40,000 pulses), at 0.5 and 0.7 J cm^{-2} laser fluences, one has been observed an increasing amount of deposited material. The double deposition timing for the 0.5 J cm^{-2} sample led to a complete cover of the Si substrates and a fine thin film formation. 40,000 laser pulses result in obtaining smother and more continuous surfaces, which form in the case of 0.7 J cm^{-2} MAPLE deposition when the transferred material starts to fill the empty places and homogenizes the morphology (Fig. 1a and b); peak to valley shortens from 927 to 660 nm and roughness improves from 132 to 97 nm.

Since the 20,000 laser pulses MAPLE deposition at 0.7 J cm^{-2} proves to be the best one, the double duration of deposition seems to confirm and even improve the morphology of the zinc benzoate thin films. Bi-dimensional morphological images of the zinc benzoate thin films, obtained by MAPLE technique at 0.7 J cm^{-2} laser fluence for 33 min (20,000 laser pulses), exhibit circular drops of around 20–25 μm diameter with increased amount of deposited material towards the edge of the circular drops (Fig. 1c). While increasing deposition time, the previously obtained circles tend to overlap and finally (for 40,000 laser pulses), homogenizing the deposited area (Fig. 1d).

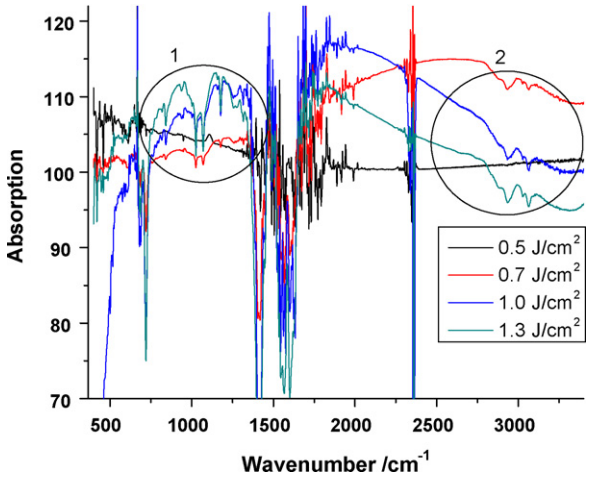

Fig. 3. FTIR spectra of zinc benzoate thin films for fluences (0.5–1.3 J cm^{-2}) that transferred significant amount of material.

The Optical Microscopy images (Fig. 2, field of view 480 μm × 360 μm) confirm the homogeneity of the deposited area for long-range domains. There is no significant difference between the two deposition durations, pointing towards 0.7 J cm^{-2} laser fluence as determinant parameter of the MAPLE deposition.

FTIR analysis of zinc benzoate thin films has been performed. For those laser fluences that were able to transfer significant amount of material (according to the AFM images), the plot of absorption *vs.* wavenumber is presented in Fig. 3. In this paper, the FTIR spectra were recorded only to check the preservation of chemical composition after the laser induced transfer.

It can be noticed that for 0.5 J cm^{-2} laser fluence the deposition is to low to be able to register the absorption signals, while for increasing laser fluences (0.7–1.3 J cm^{-2}), the peaks' amplitude increases (regions 1 and 2 in Fig. 3). The FTIR absorption peaks respect the position obtained for the bulk zinc benzoate and also to those previously reported [10,11].

4.2. Thermal analysis and kinetic decomposition studies of zinc benzoate dihydrate

Thermal analysis of $Zn(C_6H_5COO)_2{\cdot}2H_2O$ crystalline powder was carried out in both air and argon flow. Thermal decomposition

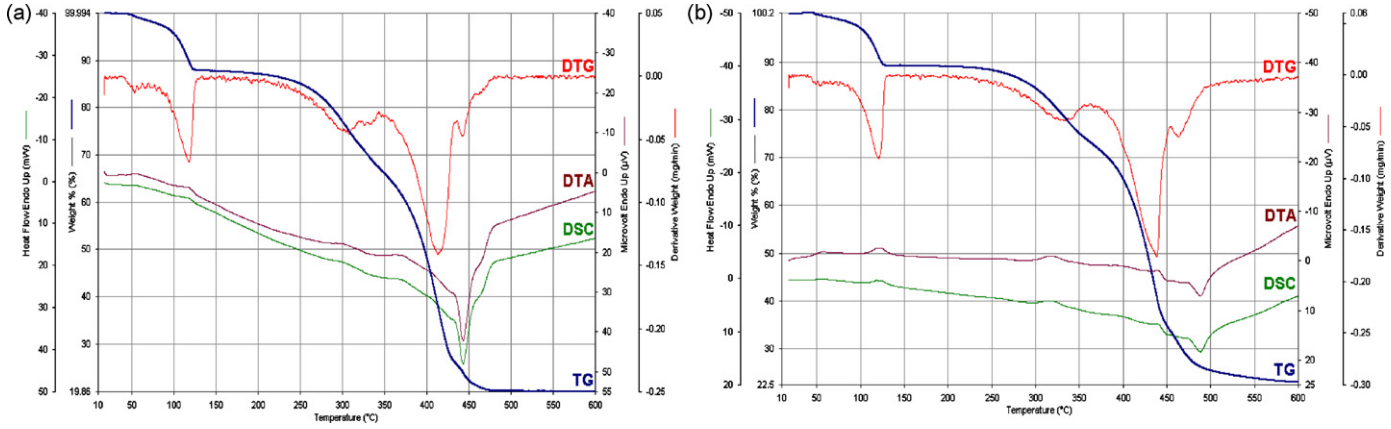

Fig. 4. Thermoanalytical curves for the thermal decomposition of $Zn(C_6H_5COO)_2{\cdot}2H_2O$ at $\beta = 10$ K min^{-1} in (a) air flow and (b) argon flow.

studies of zinc complex compounds are important from the scientific point of view, for thermal stability determinations (the case of possible biological applications) and when using them as precursors, for establishing the thermal and kinetic parameters of the decomposition process and zinc oxide growth. As it is well known from the literature, thermal decomposition and kinetics of such zinc complex crystals are determined by reacting conditions (various gaseous atmospheres) and moreover, very sensitive on the used heating rates, reacting duration and crushing pressures and durations [58–62].

The thermoanalytical curves for the non-isothermal decomposition of $Zn(C_6H_5COO)_2{\cdot}2H_2O$, recorded at the heating rate of $10\,K\,min^{-1}$ are presented in Fig. 4a (air flow) and Fig. 4b (argon flow).

Two main stages may be noticed in both air and argon flow thermal experiments, similar one to the other; the first stage represents the elimination of two coordinated water molecules (dehydration process), while the more complex second stage represents the loss of organic parts and formation of ZnO.

In the following section, a short description of some non-isothermal kinetic methods will be presented, since the current kinetic analysis requires a complex stepwise procedure for choosing and further employing them.

4.3. Non-isothermal kinetics of heterogeneous processes

Kinetic analysis of heterogeneous thermophysical processes is not only the key factor in following and understanding the investigated processes, but it has practical applications such as determining the tine-evolution of a sample behavior in other temperature conditions than it has been performed. Time consuming experiments and economical reasons (unlimited search for the best isothermal experiment, technical impossibility of using only one temperature or certain temperature programs for manufacturing, available amounts and sample costs, *etc.*) conducted frequently to the use of linear non-isothermal experiments from which kinetic parameters should be easily evaluated. The complete description of a thermophysical process is done through three kinetic parameters, the so called kinetic triplet $\{E, A, f(\alpha)\}$, where E is the activation energy, A is the pre-exponential factor, $f(\alpha)$ represents the mathematical form of the mechanism (conversion function) to be assumed for the process and α is the conversion degree. It is worth mentioning that because of three main problems to be found in the conversion rate formula (Eq. (1)):

- impossibility of separating the pre-exponential factor from the conversion function
- errors in calculating the conversion rate values from integral experiments data
- impossibility of calculating the exact value of the temperature integral and deciding which of the approximations proposed is the most reliable one

there is no unique, ultimate or even best method to be blindly applied in order to obtain the kinetic triplet

$$\frac{d\alpha}{dt} = A \cdot f(\alpha) \cdot e^{-E/RT} \tag{1}$$

Besides the three kinetic parameters, the conversion rate $(d\alpha/dt)$ formula contains also the absolute temperature (T) and universal gas constant (R).

This evaluation is usually made by various methods, like "mode-free" kinetics (E), joint model-fitting methods (single-heating rate methods) with several discrimination criteria (E, A, *sometimes* $f(\alpha)$) or by visual fitting of master plots ($f(\alpha)$). Regularly, due to their limitations, it is recommended to use more than just one method and more than just one standard procedure.

4.3.1. "Model-free" Kinetic methods (MFK)

In the case of linear non-isothermal kinetics, reviewing the single constant-heating rate methods (model-fitting methods) [63–71] led to the conclusion that they provide only erroneous results. Other papers emphasize the necessity of correlating the experiment to the kinetic predicted data and recommend the use of least squares method in order to obtain this fitting [72–75]. Budrugeac [76] analyzed the procedural errors in the kinetic triplet $\{E, A, f(\alpha)\}$ evaluation and proposed a general algorithm to be applied (standard procedure). According to this algorithm, the kinetic analysis must begin with any "mode-free" kinetic (MFK) method because they do not make assumptions on possible kinetic model form; although most of the MFK methods are isoconversional (evaluate the dependence of E on α), there were developed also other types of MFKs, like Popescu isotemperature method [77] (evaluates the dependence of E on T).

The isoconversional methods may be classified as linear (the activation energy is evaluated from the slope of a straight line) and non-linear (the activation energy is evaluated from a specific minimum condition). The isoconversional integral linear methods are based on the following integral form of the reaction rate:

$$g(\alpha) = \int_0^{\alpha} \frac{d\alpha}{f(\alpha)} = \frac{A}{\beta}\int_0^{T_\alpha} e^{-E/RT} \cdot dT = \frac{A}{\beta} I(E_\alpha, T_\alpha) \tag{2}$$

where β is the heating rate, $g(\alpha)$ is the integral conversion function and $I(E_\alpha,T_\alpha)$ represents the temperature integral. From the wide range of possibilities, in order to compare with other published results on zinc coordination compounds decompositions, we will make use of the most popular MFK method, Kissinger–Akahira–Sunose (KAS method) – integral linear method [78,79]. Substitution of $I(E_\alpha,T_\alpha)$ in Eq. (2) with Coats–Redfern approximation [80]:

$$I(E_\alpha, T_\alpha) = \frac{RT_\alpha^2}{E_\alpha} e^{-E_\alpha/RT_\alpha},$$

gives Eq. (3) – used by KAS method:

$$\ln\frac{\beta}{T^2} = \ln\frac{A \cdot R}{E \cdot g(\alpha)} - \frac{E}{R \cdot T} \tag{3}$$

Constant activation energy would describe a simple process, while its variation with conversion degree indicates complex behavior like concurrent reactions, reversible reactions or the change in limiting step [81,82].

4.3.2. Invariant kinetic parameters method (IKP)

Criado and Morales observed [83], that almost any $\alpha = \alpha(T)$ or $(d\alpha/dt) = (d\alpha/dt)(T)$ experimental curve may be correctly described by several conversion functions. The use of an integral or differential model-fitting method would lead to different activation parameters however. Although being obtained with high accuracy, the values change with different heating rates and among conversion functions. For constant isoconversional activation energies, advanced kinetic methods like invariant kinetic parameters method (IKP) are used in order to provide the pair (E_{inv},A_{inv}) [84]. As IKP method provides kinetic parameters strongly dependent on the heating rate, these results are close to the isoconversional ones only when E is independent of α.

In this paper, the chosen model-fitting method was Coats–Redfern [80] (Eq. (4)), since it is still considered to contain the best approximation of the temperature integral and is the

corresponding of KAS isoconversional method.

$$\ln\frac{g(\alpha)}{T^2} = \ln\frac{A\cdot R}{E\cdot\beta} - \frac{E}{R\cdot T} \quad (4)$$

The straight lines $\ln A_\beta$ *vs.* E_β for several constant-heating rates should intersect in a point (isoparametric point [85]) that corresponds to the true values of the activation energy and pre-exponential factor. They were named invariant kinetic parameters (E_{inv}, A_{inv}). In reality, the intersection is rather an area than a point and the range of solutions would be too wide. Considering a group of conversion functions that do not compulsory contain the true kinetic model, for each heating rate, the apparent activation parameters and corresponding compensation effect parameters (a_β and b_β) should be determined. The invariant kinetic parameters (E_{inv} and A_{inv}) are evaluated using the supercorrelation relation (Eq. (5)):

$$a_\beta = \ln A_{inv} - b_\beta\cdot E_{inv} \quad (5)$$

Invariant values are strongly dependent on the heating rates used, selected kinetic models and chosen model-fitting method.

4.3.3. Discriminating kinetic models: Perez-Maqueda et al. criterion and Master plot methods

In theory, the $f(\alpha)_{inv}$ values should be obtained by successive application of the IKP method, but in reality these values are affected by errors in ln*A* evaluation. In addition, the procedure is time-consuming and several steps induce each time supplementary errors and decrease the confidence.

Several discrimination criteria, like Perez-Maqueda et al. [86] or Master plot methods [87–94], have been proposed relying on different observations and assumptions; they may be used in order to establish the kinetic triplet or only the true conversion function.

Perez-Maqueda et al. criterion [86], also known as the criterion of kinetic parameters independence on the heating rate criterion (KPIHRC), uses the differential or any of the integral model-fitting equations – rewritten with the conversion function in the left member – against reciprocal of absolute temperature in order to obtain straight lines from which the activation parameters may be derived and the right kinetic model decided. To continue the comparisons, rewritten Coats–Redfern equation (Eq. (6)) was here employed:

$$\ln\frac{\beta\cdot g(\alpha)}{T^2} = \ln\frac{A\cdot R}{E} - \frac{E}{R\cdot T} \quad (6)$$

For each known conversion function, $\{\ln[\beta\, g(\alpha)/T^2]$ *vs.* $1/T\}$ points were plotted, while selecting the conversion degree interval, considered to be enough trustable. The right kinetic triplet is to be obtained only when all points corresponding to all employed heating rate are straight overlapping lines and the correlation coefficient has the highest value.

When several conversion functions may be situated on the same straight line and the correlation coefficients have high comparable values, the Perez-Maqueda et al. activation parameters should be compared with the invariant ones. If after using all known conversion functions there is no joint straight line to be found, then Master plot methods should be used. The Master plot method employed for the decomposition study of $Zn(C_6H_5COO)_2{\cdot}2H_2O$ uses a step by step visual fit of the normalized experimental data – $(d\alpha/dt)/(d\alpha/dt)_{max}$, by adjusting the $[f(\alpha)\ g(\alpha)]/[f(\alpha_{max})\ g(\alpha_{max})]$ master equation with the appropriate selected conversion degree and conversion function. The conversion rate data is normalized, by dividing the conversion rate values to a selected value, thus to the maximum conversion rate. Other values of α may be chosen, many papers reporting on $\alpha_{max} = 0.5$ as well [95,96]. A step by step visual fit of the normalized experimental data – $(d\alpha/dt)/(d\alpha/dt)_{max}$, by adjusting the $[f(\alpha)\, g(\alpha)]/[f(\alpha_{max})\, g(\alpha_{max})]$ master equation with the appropriate selected conversion degree and conversion function, is the main advantage in determining the true kinetic model for each constant heating rate experiment.

4.4. Dehydration of $Zn(C_6H_5COO)_2{\cdot}2H_2O$

As a consequence of zinc benzoate solubility in water [11], anhydrous zinc benzoate easily coordinates two water molecules (~12% in $Zn(C_6H_5COO)_2{\cdot}2H_2O$) and retains additional absorbed water. For the first decomposition stage, approximately 3% of the water solvent in both gaseous atmospheres (constant endothermic loss of 0.45% min^{-1} from 40 to 85 °C) are firstly eliminated. The maximum decomposition rate for the elimination of the two crystallization water molecules happens around 118 °C in both cases (~4.35% min^{-1}). The dehydration process ends at 128 °C (air and argon flow), being similar to the dehydration of zinc acetate dihydrate [58,59].

It can be seen from the DTG curves (Fig. 3) that the dehydration of $Zn(C_6H_5COO)_2{\cdot}2H_2O$ is a single step process, the loss of both coordinated water molecules happening simultaneously. Same behavior was noticed by Locatelli et al. for the thermal decomposition of trihydrated lanthanum benzoate [97], while other hydrated lanthanide and yttrium benzoates are gradually loosing the coordinated water molecules. Terakita and Byrn [98] studied the structure and physical stability of hydrates and thermotropic mesophase of calcium benzoate and noticed continuous loss of water in both trihydrate and monohydrate cases, the monohydrate decomposing slower because of the better bonding. However, calcium benzoate trihydrate dehydration is sensitive to grinding, splitting the process firstly in losing two molecules, followed at high temperatures by the elimination of the remained coordinated water molecule.

Up to now, there has been no kinetic study of the dehydration and decomposition of benzoates, therefore the comparison will be made only with respect to the dehydration kinetics of similar compounds (*i.e.* $Zn(CH_3COO)_2{\cdot}2H_2O$). Duan et al. [59] used for the dehydration process of $Zn(CH_3COO)_2{\cdot}2H_2O$ the method proposed by Tang et al. [99], which provides very close results [100] to KAS method, as they relay on very close equations. Friedmann method [101], used by Koga and Tanaka [58] for the same dehydration process, provided trustable enough values for the isoconversional activation energy, as revealed by the reported error values.

While Koga and Tanaka [58] carried out a systematic study on thermal dehydration of $Zn(CH_3COO)_2{\cdot}2H_2O$ (single crystals and crushed crystals of various fractions of particle size), Duan et al. [59] limited their kinetic study only to one sample, which was previously gently crushed, but without indicating the particles' size.

In order to have an efficient comparison, the isoconversional activation energy for the dehydration process of $Zn(C_6H_5COO)_2{\cdot}2H_2O$ was evaluated by means of KAS "model-free" kinetic method [78,79]. This method seems to be the most appropriate in following the activation energy trend for complex processes and is independent of instantaneous changes (the case of "local linear" method of Tang and Chen [102] or "average linear" method of Ortega [103]) and on reaction rate fluctuations (the case of Friedmann method [101]).

Thus, for α = const., the plot $\ln(\beta/T^2)$ *vs.* $(1/T)$, obtained from the experimental thermogravimetric curves recorded for several constant-heating rates, should be a straight line whose slope could be used for the activation energy evaluation. Fig. 5 presents the activation energy behavior during the entire elimination of water molecules (air flow, but same results have been obtained for the argon flow experiments); it increases from ~120 to 152 kJ mol^{-1}, its shape being alike to the dehydration of $Zn(CH_3COO)_2{\cdot}2H_2O$ single crystals [58]. As the reaction occurs under relatively high water vapor pressures, the increase in activation energy may be explained by a change in the self-generated water vapor concentration at the

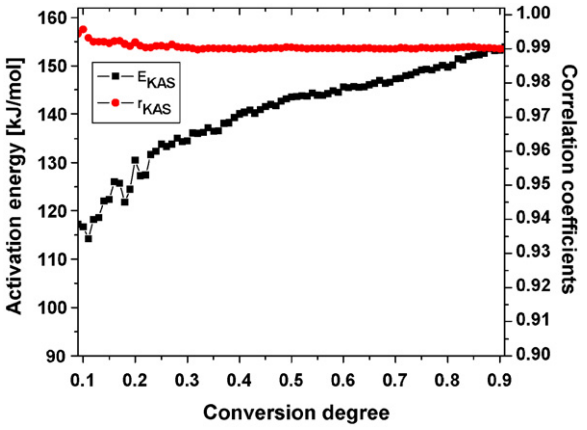

Fig. 5. Isoconversional activation energy for the dehydration process of $Zn(C_6H_5COO)_2{\cdot}2H_2O$.

reaction interface [58] and better bonding of the remained coordinated water molecules.

Even if the isoconversional activation energy is not constant during the consumption of the dehydration reaction, it would be valuable to check if only one kinetic model applies, since there should be only one chemical mechanism occurring. Normalized reaction rates were found to have maxima at $\alpha = 0.77$ for all experiments. The Master plot method presented in Section 4.3 provide two kinetic models as simultaneously describing the process (D4 and F1/2 – same with R2). Perez-Maqueda et al. criterion by using Coats–Redfern equation ($\alpha = 0.2$–0.8) provides straight overlapping lines only for D4 kinetic model and the following activation parameters: $E_{PM} = 150.6\,kJ\,mol^{-1}$, $\ln A = 40.400\ (A/s^{-1})$ obtained with $r = 0.99192$.

For Perez-Maqueda et al., the activation energy is comprised in the range of isoconversional energies (that indicate changing kinetic mechanism), the independency of activation parameters principle on the heating rate applying only in the case of D4 kinetic model which becomes determinant for the transformation rate, therefore in Fig. 6 only the D4 fit is presented.

4.5. Decomposition of $Zn(C_6H_5COO)_2$ and formation of ZnO

Thermal decomposition of zinc benzoate is a complex process, in argon flow and even more complex in air flow (Fig. 4). While in argon the decomposition occurs in three steps (Fig. 4b) – first two endothermic and the third exothermic, in air flow the first and the third step are initiated by gaseous oxygen and continued by the oxygen from inside the organic molecules (Fig. 4a), when the

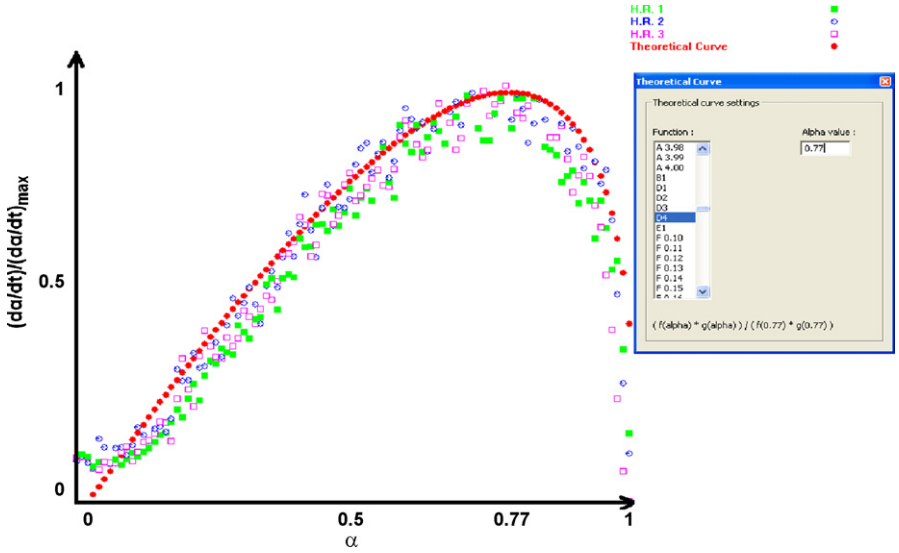

Fig. 6. Master plot method for the dehydration process of $Zn(C_6H_5COO)_2{\cdot}2H_2O$.

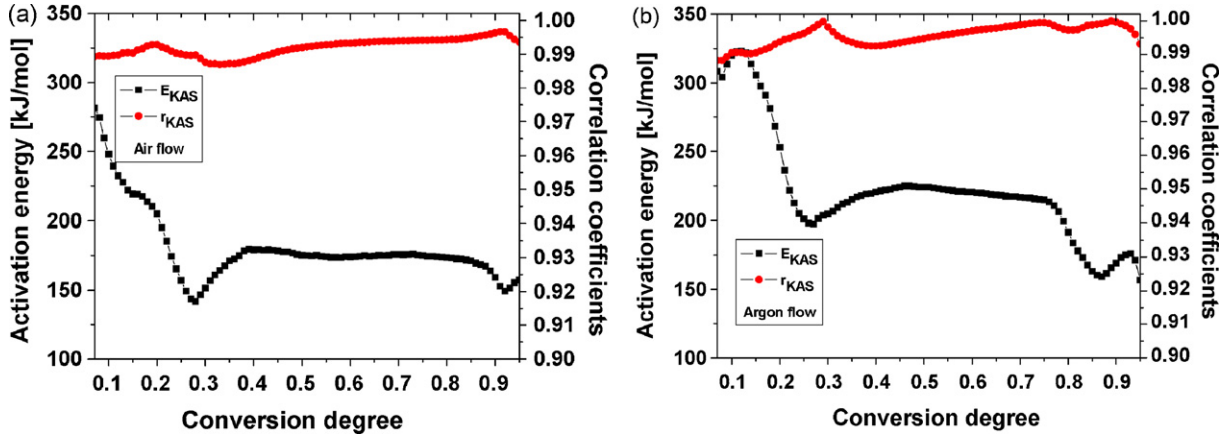

Fig. 7. Isoconversional activation energy for the non-isothermal decomposition process of $Zn(C_6H_5COO)_2$ in (a) air flow and in (b) argon flow.

Table 2
Apparent activation parameters by CR equation for each constant-heating rate; air flow case.

Kinetic model	$\beta = 2.08\ K\ min^{-1}$			$\beta = 6.30\ K\ min^{-1}$			$\beta = 10.54\ K\ min^{-1}$		
	$E\ (kJ\ mol^{-1})$	$\ln A\ (A/s^{-1})$	r	$E\ (kJ\ mol^{-1})$	$\ln A\ (A/s^{-1})^1$	r	$E\ (kJ\ mol^{-1})$	$\ln A\ (A/s^{-1})$	r
F0.10	55.1	2.347	0.99936	49.1	1.955	0.99900	52.5	2.892	0.99910
F0.15	56.9	2.751	0.99928	50.9	2.323	0.99891	54.4	3.274	0.99902
F0.20	58.9	3.179	0.99920	52.6	2.701	0.99882	56.2	3.652	0.99893
F0.25	60.8	3.590	0.99911	54.4	3.074	0.99872	58.1	4.048	0.99884
F0.30	62.8	4.011	0.99902	56.2	3.464	0.99862	60.0	4.446	0.99874
A3.00	24.8	−3.651	0.99911	21.5	−3.468	0.99890	23.2	−2.699	0.99894
A3.10	23.6	−3.930	0.99914	20.4	−3.707	0.99893	22.1	−2.948	0.99898
A3.20	22.6	−4.164	0.99917	19.4	−3.935	0.99897	21.0	−3.186	0.99901
A3.30	21.5	−4.410	0.99919	18.6	−4.145	0.99900	20.1	−3.403	0.99904
A3.40	20.6	−4.622	0.99922	17.7	−4.353	0.99903	19.1	−3.617	0.99907
A3.50	19.7	−4.830	0.99924	16.8	−4.557	0.99906	18.3	−3.814	0.99910
A3.60	18.9	−5.035	0.99926	16.1	−4.744	0.99908	17.5	−4.004	0.99912
A3.70	18.0	−5.247	0.99928	15.4	−4.916	0.99911	16.7	−4.196	0.99915
A3.80	17.3	−5.425	0.99930	14.7	−5.090	0.99913	16.0	−4.363	0.99917
A3.90	16.6	−5.587	0.99932	14.0	−5.252	0.99916	15.2	−4.540	0.99919
A4.00	15.9	−5.754	0.99934	13.4	−5.404	0.99918	14.5	−4.707	0.99921
P0.50	113.8	13.508	0.99903	102.6	11.901	0.99837	109.3	13.198	0.99855
P1.00	51.5	1.566	0.99950	45.9	1.250	0.99917	49.1	2.166	0.99926
P1.50	30.7	−2.663	0.99966	26.9	−2.576	0.99944	28.9	−1.779	0.99950
P2.00	20.4	−4.925	0.99975	17.5	−4.643	0.99959	18.9	−3.908	0.99963
P2.50	14.2	−6.399	0.99980	11.8	−6.023	0.99967	12.9	−5.321	0.99970
P3.00	10.0	−7.486	0.99984	8.0	−7.052	0.99973	8.9	−6.375	0.99976

system becomes activated and releases the intramolecular oxygen. The DSC and DTA curves in air flow identify the same first two endothermic reactions and split the third reaction into two exothermic steps.

The three reactions are similar to those proposed by several authors [59–62] for the thermal decomposition in inert dynamic atmosphere of zinc acetate:

$$3/4Zn(C_6H_5COO)_2 \rightarrow 3/16(C_6H_5CO)_2O\uparrow + 3/16Zn_4O(C_6H_5COO)_6 \quad (R1)$$

$$3/16Zn_4O(C_6H_5COO)_6 \rightarrow 3/4ZnO + 9/16(C_6H_5)_2CO\uparrow + 9/16CO_2\uparrow \quad (R2)$$

$$1/4Zn(C_6H_5COO)_2 \rightarrow 1/4ZnO + 7/2CO_2\uparrow + 5/2H_2O\uparrow \quad (R3)$$

The first reaction represents the loss of $(C_6H_5CO)_2O$ (15% mass loss) and the formation of $Zn_4O(C_6H_5COO)_6$, stable at those temperatures. This reaction represents only 3/4 of the decomposition of zinc benzoate, while the second reaction (42% mass loss) represents the decomposition of solid $Zn_4O(C_6H_5COO)_6$ to the more stable ZnO and happens in a narrow temperature range. The rest of 1/4 ZnO forms at the end of the third reaction, when the high temperatures led to the combustion of organic gases to CO_2 and H_2O. A residue of 22% representing ZnO is found for the argon flow case, while in the case of air flow only 20% remain.

Fig. 7 shows the variation in activation energy with the conversion degree towards the formation of ZnO from the thermal decomposition of zinc benzoate, in air and in argon flow respectively. The evaluation was made using the TKS-SP software [100,104], with α step of 0.01, while obtaining the activation energy with correlation coefficients greater than 0.98800 for both air and argon studies.

Table 3
Apparent activation parameters by CR equation for each constant-heating rate; argon flow case.

Kinetic model	$\beta = 2.02\ K\ min^{-1}$			$\beta = 6.12\ K\ min^{-1}$			$\beta = 10.22\ K\ min^{-1}$		
	$E\ (kJ\ mol^{-1})$	$\ln A\ (A/s^{-1})$	r	$E\ (kJ\ mol^{-1})$	$\ln A\ (A/s^{-1})$	r	$E\ (kJ\ mol^{-1})$	$\ln A\ (A/s^{-1})$	r
F0.10	65.4	3.753	0.99940	71.2	5.551	0.99940	59.8	3.803	0.99970
F0.15	67.0	4.080	0.99937	73.0	5.909	0.99935	61.4	4.123	0.99965
F0.20	68.7	4.444	0.99932	74.9	6.291	0.99929	63.090	4.454	0.99960
F0.25	70.5	4.801	0.99926	76.8	6.657	0.99923	64.7	4.784	0.99955
F0.30	72.5	5.211	0.99921	78.8	7.058	0.99918	66.3	5.104	0.99949
A3.00	26.3	−3.678	0.99939	28.9	−2.232	0.99936	23.2	−2.980	0.99949
A3.10	24.9	−3.976	0.99941	27.5	−2.521	0.99938	22.2	−3.194	0.99951
A3.20	23.9	−4.201	0.99943	26.3	−2.770	0.99940	21.1	−3.420	0.99952
A3.30	22.8	−4.447	0.99945	25.1	−3.015	0.99942	20.1	−3.646	0.99953
A3.40	21.8	−4.672	0.99946	24.0	−3.258	0.99944	19.2	−3.860	0.99955
A3.50	20.8	−4.886	0.99948	23.1	−3.456	0.99945	18.3	−4.055	0.99956
A3.60	19.9	−5.095	0.99949	22.2	−3.653	0.99947	17.4	−4.249	0.99957
A3.70	19.2	−5.268	0.99951	21.2	−3.857	0.99948	16.7	−4.417	0.99959
A3.80	18.4	−5.450	0.99952	20.3	−4.068	0.99949	16.0	−4.584	0.99960
A3.90	17.6	−5.633	0.99953	19.5	−4.232	0.99951	15.3	−4.752	0.99961
A4.00	16.9	−5.795	0.99955	18.7	−4.417	0.99952	14.5	−4.933	0.99962
P0.50	135.2	16.379	0.99907	146.6	18.795	0.99903	125.0	15.168	0.99960
P1.00	62.0	3.058	0.99952	67.5	4.827	0.99949	56.7	3.183	0.99980
P1.50	37.6	−1.631	0.99967	41.3	−0.039	0.99966	34.0	−1.066	0.99987
P2.00	25.6	−4.069	0.99977	28.0	−2.647	0.99974	22.5	−3.349	0.99990
P2.50	18.2	−5.669	0.99981	20.1	−4.285	0.99980	15.7	−4.823	0.99992
P3.00	13.2	−6.841	0.99984	14.9	−5.453	0.99983	11.2	−5.914	0.99994

Table 4
Compensation effect parameters for all selected kinetic models by CR method.

β (K min^{-1})	Atmosphere	a_β (A/s^{-1})	b_β (mol J^{-1})	r
2.08	Air flow	−8.87984	2.01×10^{-4}	0.96243
6.30		−7.98146	1.99×10^{-4}	0.95480
10.54		−7.43173	1.94×10^{-4}	0.95788
2.02	Argon flow	−8.88552	1.91×10^{-4}	0.96806
6.12		−7.73714	1.87×10^{-4}	0.95783
10.22		−7.47330	1.86×10^{-4}	0.96126

For the argon flow experiments, the first reaction have a decreasing activation energy from 320 to 180 kJ mol^{-1} (at $\alpha = 0.28$), followed by a small increase in activation energy up to 210 kJ mol^{-1} (at $\alpha = 0.35$) – Fig. 7b. In air flow, the reaction initiates with the oxygen from the air, results in the activation energy being lower. This time decreasing from 270 to 135 kJ mol^{-1} (at $\alpha = 0.28$); it is followed by a severe increase to 170 kJ mol^{-1} (once more at $\alpha = 0.35$) for the intramolecular oxygen reaction – Fig. 7a.

The beginning of the second reaction at $\alpha = 0.35$ (start of constant activation energy) in both cases indicates that the first reaction offered the same products in the end, independently on the source of consumed oxygen. As well, being constant in the range of $\alpha = 0.35$–0.85 (air flow) and between $\alpha = 0.35$ and 0.75 (argon flow), the activation energy indicates together with the DTG curve a simple process for the second reaction: $\bar{E}_{KAS} = 175$ kJ mol^{-1} (air flow) and $\bar{E}_{KAS} = 215$ kJ mol^{-1} (argon flow). The difference in activation energy of the second reaction may be explained as a supplementary effort the system has to surpass in the absence of external oxygen (argon flow) in order to complete the reaction. Since the activation energy of the third reaction in argon flow is lower and even decreasing, it begins earlier, at $\alpha = 0.75$. The shape of the activation energy variation of the third reaction is similar for both air and argon flows, indicating the same reaction, regardless of atmosphere; thus independent of implied oxygen. As well, its profile is almost identical to the first reaction one, the trough-like shape being one more indication of zinc benzoate decomposition.

Since the activation energy of the second reaction remains constant, it would be possible to evaluate the entire kinetic triplet. For each type of employed atmospheres, it was possible to make use of Coats–Redfern (CR) equation and calculate the apparent activation parameters for each constant-heating rate (air flow – Table 2 and argon flow – Table 3). Even if the conversion degree values are apparent as well, the contraction or dilatation of the employed range should not create problems in the evaluation. For the air flow case we have used $\alpha = 0.35$–0.85 range and for the argon flow case $\alpha = 0.35$–0.75 range.

As it has been previously described in Section 4.3.2, for each heating rate the compensation effect parameters may be evaluated; Table 4 contains the compensation effect parameters (a_β,b_β) values, for when all selected kinetic models (ASKM) from Tables 2 and 3 have been gathered.

Table 5
Invariant kinetic parameters for ASKM by CR method.

Atmosphere	E_{inv} (kJ mol^{-1})	ln A_{inv} (A/s^{-1})	r_{inv}
Air flow	174.1	26.414	0.97583
Argon flow	212.2	31.412	0.97612

Table 6
Perez-Maqueda et al. kinetic parameters by CR method.

Atmosphere	Kinetic model	E (kJ mol^{-1})	ln A (A/s^{-1})	r
Air flow	P1/3	175.3	24.955	0.99366
Argon flow	P1/3	218.8	31.185	0.99629

The results of IKP method (Table 5) are identical with the average values of isoconversional activation energies by KAS method, although obtained with less confidence.

Due to the complex process (three chemical reactions), the Master plot method require the exact knowledge of initial and final conversion degrees and therefore cannot be used in this case. Perez-Maqueda et al. criterion can discriminate between conversion functions, even using only parts of the process. Since the complexity of the process is not suitable for kinetic predictions, this criterion is powerful enough to indicate the activation parameters (E,A) and can prove their constancy with respect to the heating rates.

Table 6 presents the kinetic parameters of the second reaction within the process, obtained with increased accuracy. The activation energies are those expected and the conversion function remains the same for both types of experiments. The obtaining of unchanged conversion function with the employed atmosphere is a great achievement, to be discussed in the followings.

4.6. Obtaining ZnO by thermal treatment of the zinc benzoate thin films

In order to obtain thin films of ZnO by thermally decomposing zinc benzoate, thermal analysis and comparative decomposition kinetic study of the precursor in air and argon flow atmospheres have been carried out. The thermal analysis indicate that a oxygen enriched atmosphere favor the formation at lower temperatures of ZnO, while the kinetic study indicate that the same oxygen enriched atmosphere decreases the activation energy of each thermal-induced decompositions. While the shape of isoconversional activation energy is practically the same, for the constant values (corresponding to the second reaction) a compensation effect behavior may be noticed between the two different atmospheres (Tables 5 and 6); this means same chemical decomposition pathway undergoing, and where possible to evaluate the kinetic triplet, the kinetic mechanism seems not changing as well (power law $n = 1/3$).

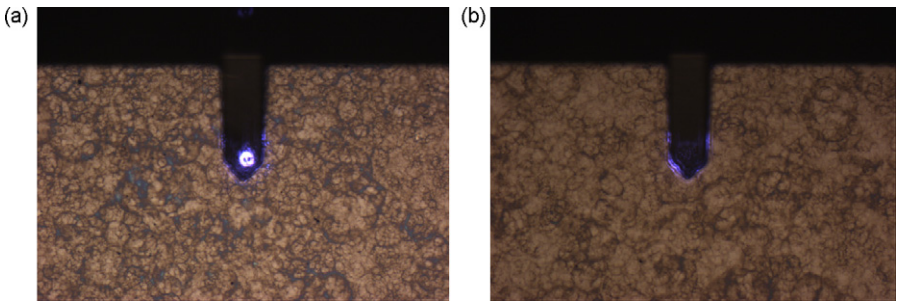

Fig. 8. Optical microscopy images of the thermally treated zinc benzoate thin films by MAPLE, obtained at 0.7 J cm^{-2} laser fluence (a) 20,000 pulses and (b) 40,000 pulses.

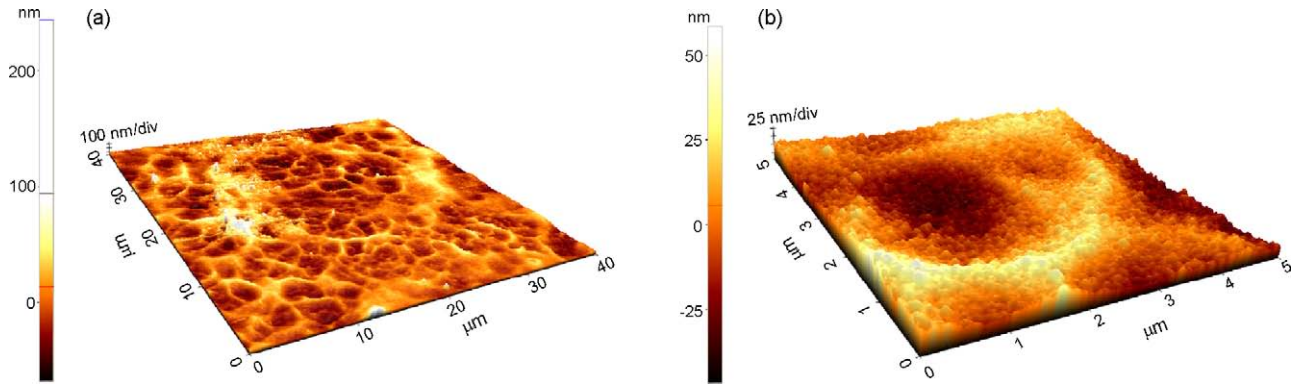

Fig. 9. 3D AFM images of the thermally treated zinc benzoate thin films by MAPLE, obtained at 0.7 J cm^{-2} laser fluence and 20,000 pulses; (a) 40 μm × 40 μm area and (b) 5 μm × 5 μm area (5 times magnified on the height axis).

Translated to the need of obtaining reproducible decomposition pathways, by knowing their kinetics and by controlling the kinetic parameters, the gaseous atmosphere is still an important parameter, but not limitative for the purpose of obtaining reproducible ZnO thins films. However an oxygen enriched atmosphere lowers the activation of decomposition process and shifts the processes to lower temperatures, in this case needed for enhancing the thermal treatment of as many as possible types of "deposited layer + substrates" systems. Lower temperatures and lower heating rates are recommended thus to be used for obtaining ZnO this films from complex zinc precursor, the chemical and the microscopic structure of the substrate or the compatibility between the layers and the substrates, remain unchanged.

The thin films of $Zn(C_6H_5COO)_2$ obtained by MAPLE technique have been thermally treated in static air atmosphere inside a muffle furnace, from room temperature up to 650 °C with the heating rate of 1 K min^{-1}. In Fig. 8 we present the optical microscopy images of the thin films after thermal treatment, previously deposited with 0.7 J cm^{-2} laser fluence, for 20,000 pulses (Fig. 8a) and respectively 40,000 pulses (Fig. 8b). It is clearly shown that a brighter image for the lowest deposition timing (Fig. 8a), while doubling it gives the ZnO thin film a higher coating degree on the Si substrates (Fig. 8b).

Detailed AFM images after thermal treatment (obtained for 0.7 J cm^{-2} and 20,000 pulses) in Fig. 9 are 5 times magnified on the height axis in order to observe the microscopic array of the ZnO structures. The thin films are smooth and uniform, possessing a constant local ZnO distribution (similar anisotropic grains close-packed) [105], but a long-range one as well (overlapped circular domains).

After thermal treatment, the thin films become much smoother, peak to valley (R_{P-V}) reducing 3 times from 927 to 312 nm and roughness (R_Q) decreasing 5.5 times from 132 to 23 nm. This result is in accordance with the ~20% ZnO that remain as final product of the thermal decomposition.

5. Conclusions

Zinc benzoate thin films have been obtained by MAPLE technique, in order to use them as already deposited precursors for ZnO thin films manufacture, as it was found the final product of its thermal decomposition. A comparative study of 1% zinc benzoate frozen solution in methanol was carried out for several fluences and two deposition durations. Comparative thermal analysis and non-isothermal kinetic investigation of $Zn(C_6H_5COO)_2{\cdot}2H_2O$ dehydration and decomposition was performed. Thin films morphology and chemical preservation have been investigated by AFM and FTIR spectroscopy. The dehydration process is described by slightly increasing activation energy and diffusion controlled mechanism, as it occurs under relatively high water vapor pressures with change in the self-generated water vapor concentration at the reaction interface. The decomposition of $Zn(C_6H_5COO)_2$ is a three-reaction process, initiating reactions being controlled by the oxygen concentration in the flowing gases. Activation parameters present compensating effect behaviour, with increased activation energy for the inert atmosphere reactions. Even if the reactions' consumption is controlled by oxygen concentration, the kinetic pathway preserves. For obtaining ZnO thin films from zinc benzoate precursor, it can be concluded that the concentration of oxygen is not limitative for the chemical reactions, but limitative only for the temperature ranges they happen. ZnO has been obtained by thermal treatment the obtained thin films, according to the thermal analysis and decomposition kinetics of zinc benzoate; smooth and uniform ZnO thin films have homogeneous local distribution (similar anisotropic grains close-packed), but a long-range one as well (overlapped circular domains).

Acknowledgments

The authors are grateful to A. Erdelyiova and Z. Budjovska for contributing to the zinc benzoate synthesis and to Dr N. Scărişoreanu for the help he provided during the MAPEL deposition. A. Rotaru acknowledges Dr G. Epurescu, Dr D. Arnold and C. Kavanagh for the useful discussions.

References

[1] J.M. Berg, Y. Shi, Science 27 (1996) 1081.
[2] Y. Anjaneyulu, N.B. Raman, R.P. Rao, Ind. J. Microbiol. 25 (1985) 125.
[3] D. Stefanitsi, J.R. Garel, Lett. Appl. Microbiol. 24 (1997) 180.
[4] J.E. Coleman, Ann. Rev. Biophys. Biomol. Struct. 21 (1992) 441.
[5] I. Fridovich, Science 201 (1978) 875.
[6] T.J. Beveridge, R.J. Doyle, Metal Ions and Bacteria, John Wiley and Sons, New York, 1989.
[7] A. Holm, H.D. Poulsen, Compend. Contin. Educ. Pract. Vet. 18 (1996) 26.
[8] E. Szunyogova, D. Mudronova, K. Gyoryova, R. Nemcova, J. Kovarova, L. Piknova-Findorakova, J. Therm. Anal. Calorim. 88 (2007) 355.
[9] K.B. Diehl, Am. Fam. Physician 54 (1996) 171.
[10] J. Skorsepa, E. Godocikova, J. Cernak, J. Therm. Anal. Calorim. 75 (2004) 773.
[11] L. Findorakova, K. Gyoryova, J. Kovarova, V. Balek, F.A. Nour El-Dien, L. Halas, J. Therm. Anal. Calorim. 95 (2009) 923–928.
[12] Z.R. Tian, J.A. Voigt, J. Liu, B. McKenzie, M.J. McDermott, M.A. Rodriguez, H. Konishi, H. Xu, Nat. Mater. 2 (2003) 821.
[13] P. Gerstel, R.C. Hoffmann, P. Lipowsky, L.P.H. Jeurgens, J. Bill, F. Aldinger, Chem. Mater. 18 (2005) 179.
[14] L.P. Bauermann, J. Bill, F. Aldinger, J. Phys. Chem. B 110 (2006) 5182.
[15] C. Liewhiran, S. Seraphin, S. Phanichphant, Curr. Appl. Phys. 6 (2006) 499.
[16] Y. Yang, H. Chen, B. Zhao, X. Bao, J. Cryst. Growth 263 (2004) 447.
[17] A. Somwangthanaroj, K. Sunwanchatchai, S. Ando, W. Tanthapanichakoon, Mater. Chem. Phys. 114 (2009) 751.
[18] H. Makino, A. Miyake, T. Yamada, N. Yamamoto, T. Yamamoto, Thin Solid Films 517 (2009) 3138.
[19] A. Rotaru, C. Constantinescu, P. Rotaru, A. Moanta, M. Dumitru, M. Socaciu, M. Dinescu, E. Segal, J. Therm. Anal. Calorim. 92 (2008) 279.

[20] C. Constantinescu, A. Palla-Papavlu, A. Rotaru, P. Florian, F. Chelu, M. Icriverzi, A. Nedelcea, V. Dinca, A. Roseanu, M. Dinescu, Appl. Surf. Sci. 255 (2009) 5491.
[21] G. Epurescu, G. Dinescu, A. Moldovan, R. Birjega, F. Dipietrantonio, E. Verona, P. Verardi, L.C. Nistor, C. Ghica, G. Van Tendeloo, A. Dinescu, M. Dinescu, Superlattice Microst. 42 (2007) 79.
[22] Y. Yan, S.B. Zhang, Phys. Rev. Lett. 86 (2001) 5723.
[23] M. Joseph, H. Tabata, T. Kawai, Jpn. J. Appl. Phys. 38 (1999) L1205.
[24] R.J. Mendelsberg, M. Kerler, S.M. Durbin, R.J. Reeves, Superlattice Microst. 43 (2008) 594.
[25] B.L. Zhu, X.Z. Zhao, F.H. Su, G.H. Li, X.G. Wu, J. Wu, R. Wu, J. Liu, Physica B 396 (2007) 95–101.
[26] A. Fouchet, W. Prellier, B. Mercey, L. Mechin, V.N. Kulkarni, T. Venkatesan, J. Appl. Phys. 96 (2004) 3228.
[27] D. Anglos, A. Stassinopoulos, R.N. Das, G. Zacharakis, M. Psyllaki, R. Jakubiak, R.A. Vaia, E.P. Giannelis, S.H. Anastasiadis, J. Opt. Soc. Am. B 21 (2004) 208.
[28] A. Stassinopoulos, R.N. Das, E.P. Giannelis, S.H. Anastasiadis, D. Anglos, Appl. Surf. Sci. 247 (2005) 18.
[29] R.A. McGill, R. Chung, D.B. Chriesy, P.C. Dorsey, P. Matthews, A. Pique, T.E. Mlsna, J.L. Stepnowski, IEEE T. Ultrason. Ferr. Freq. Control 45 (1998) 1370.
[30] A. Pique, R.A. McGill, D.B. Chrisey, D. Leonhardt, T.E. Mslna, B.J. Spargo, J.H. Callahan, R.W. Vachet, R. Chung, M.A. Bucaro, Thin Solid Films 355–356 (1999) 536.
[31] D.B. Chrisey, A. Pique, R.A. McGill, J.S. Horwitz, B.R. Ringeisen, D.M. Bubb, P.K. Wu, Chem. Rev. 103 (2003) 553.
[32] V. Musat, P. Budrugeac, R.C.C. Monteiro, E. Fortunato, E. Segal, J. Therm. Anal. Calorim. 89 (2007) 505.
[33] P. Budrugeac, V. Musat, E. Segal, J. Therm. Anal. Calorim. 89 (2007) 699.
[34] Y.N. Chang, J.H. Hsieh, C.N. Wang, L.T. Hong, in: B.D. Weaver, O.M. Manasreh, C. Jagadish, S. Zollner (Eds.), Progress in Semiconductors II-Electronic and Optoelectronic Applications, Book Series: Materials Research Society Symposium Proceedings, 744 (2003) 187.
[35] N. Audebrand, J.P. Auffredic, D. Louer, Chem. Mater. 10 (1998) 2450.
[36] X.Y. Zhao, C.Z. Li, B.C. Zheng, L.M. Hu, H.C. Gu, S.C. Zhang, 96 China-Japan Symposium on Particuology Proceedings, 1996, p. 137.
[37] J. Cunningham, M. Oneill, G. Patrick, N. Hickey, Z. Wang, A.K. Galway, J.L.G. Fierro, J. Therm. Anal. 41 (1994) 651.
[38] Z. Li, X. Shen, X. Feng, P. Wang, Z. Wu, Thermochim. Acta 438 (2005) 102.
[39] M.J. Madou, Fundamentals of Microfabrication. The Science of Miniaturization, Second edition, CRC Publisher, 2002, 168.
[40] M. Lambrechts, W. Sansen, Biosensors: Microelectrochemical Devices, The Institute of Physics Publishing, 1992.
[41] S. Aquaviva, M. Fernandez, G. Leggieri, A. Luches, M. Martino, A. Perrone, Appl. Phys. A Mater. Sci. Process. 69 (1999) S471.
[42] Solar Thin Films Company, http://www.solarthinfilms.com/active/en/home.html.
[43] N.M. Sbrockey, J.D. Cuchiaro, B.H. Hoerman, L.G. Provost, C.E. Rice, S. Sun, G.S. Tompa, S. Ganesan, J. Nause, W.B. Nemeth, III–Vs Review Adv. Semicond. Magn. 17 (2004).
[44] M. Jelinek, J. Remsa, E. Brynda, M. Houska, T. Kocourek, Appl. Surf. Sci. 254 (2007) 1240.
[45] F. Bloisi, A. Cassinese, R. Papa, L. Vicari, V. Califano, Thin Solid Films 516 (2008) 1594.
[46] K. Rodrigo, P. Czuba, B. Toftmann, J. Schou, R. Pedrys, Appl. Surf. Sci. 252 (2006) 4824.
[47] B. Toftmann, K. Rodrigo, J. Schou, R. Pedrys, Appl. Surf. Sci. 247 (2005) 211.
[48] D.M. Bubb, R.A. McGill, J.S. Horwitz, J.M. Fitz-Gerald, E.J. Houser, R.M. Stroud, P.W. Wu, B.R. Ringeisen, A. Pique, D.B. Chrisey, J. Appl. Phys. 89 (2001) 5739.
[49] D.M. Bubb, B.R. Ringeisen, J. Callahan, M. Galicia, A. Vertes, J.S. Horwitz, R.A. McGill, E.J. Houser, P.K. Wu, A. Pique, D.B. Chriesy, Appl. Phys. A 73 (2001) 121.
[50] C. Constantinescu, N. Scarisoreanu, A. Moldovan, M. Dinescu, C. Vasiliu, Appl. Surf. Sci. 253 (2007) 7711.
[51] A. Rotaru, A. Kropidlowska, C. Constantinescu, N. Scarisoreanu, M. Dumitru, M. Strankowski, P. Rotaru, V. Ion, C. Vasiliu, B. Becker, M. Dinescu, Appl. Surf. Sci. 255 (2009) 6786.
[52] E. Leveugle, L.V. Zhigilei, A. Sellinger, J.M. Fitz-Gerald, J. Phys. Conf. Ser. 59 (2007) 126.
[53] L.V. Zhigilei, B.J. Garrison, Appl. Phys. A Mater. Sci. Process. 69 (1999) S75.
[54] E. Leveugle, L.V. Zhigilei, J. Appl. Phys. 102 (2007) 074914–74921.
[55] A.T. Sellinger, E. Leveugle, K. Gogick, G. Peman, L.V. Zhigilei, J.M. Fitz-Gerald, J. Phys. Conf. Ser. 59 (2007) 314.
[56] Y.G. Yingling, L.V. Zhigilei, B.J. Garrison, A. Koubenakis, J. Labrakis, S. Georgiou, Appl. Phys. Lett. 78 (2001) 1631.
[57] L.V. Zhigilei, Appl. Phys. A Mater. Sci. Process. 76 (2003) 339.
[58] N. Koga, H. Tanaka, Thermochim. Acta 303 (1997) 69.
[59] Y. Duan, J. Li, X. Yang, L. Hu, Z. Wang, Y. Liu, C. Wang, J. Anal. Appl. Pyrol. 83 (2008) 1–6.
[60] T. Arri, A. Kishi, Thermochim. Acta 373 (2003) 22.
[61] H.G. McAdie, J. Inorg. Nucl. Chem. 28 (1966) 2801.
[62] D.X. Tang, Y. Zhao, Chin. J. Chem. Phys. 16 (2003) 237.
[63] M.E. Brown, M. Maciejewski, S. Vyazovkin, R. Nomen, J. Sempere, A.K. Burnham, J. Opfermann, R. Strey, H. Andreson, A. Kemmler, R. Keuleers, J. Jannsens, H.O. Desseyn, C.R. Li, T.B. Tang, B. Roduit, J. Malek, T. Mitsuhasni, Thermochim. Acta. 355 (2000) 125.
[64] B. Roduit, Thermochim. Acta. 355 (2000) 171.
[65] S. Vyazovkin, Thermochim. Acta. 355 (2000) 155.
[66] M. Maciejewski, Thermochim. Acta. 355 (2000) 145.
[67] G. Varhegyi, J. Anal. Appl. Pyrol. 79 (2007) 278.
[68] M. Maciejewski, S. Vyazovkin, Thermochim. Acta 370 (2001) 149.
[69] L.A. Perez-Maqueda, J.M. Criado, P.E. Sanchez-Jimenez, J. Phys. Chem. A 110 (2006) 12456.
[70] A. Rotaru, A. Moanta, P. Rotaru, E. Segal, J. Therm. Anal. Calorim. 95 (2009) 161.
[71] A. Rotaru, G. Bratulescu, P. Rotaru, Thermochim. Acta 489 (2009) 61.
[72] A.K. Burnham, R.L. Braun, Energy Fuels 13 (1999) 1.
[73] J.A. Conesa, A. Marcilla, J.A. Cabalerro, R. Font, J. Anal. Appl. Pyrol. 58/59 (2001) 617.
[74] J.A. Cabalerro, J.A. Conesa, J. Anal. Appl. Pyrol. 73 (2005) 85.
[75] J. Cai, R. Liu, Bioresour. Technol. 99 (2008) 2795.
[76] P. Budrugeac, Polym. Degrad. Stab. 89 (2005) 265.
[77] C. Popescu, Thermochim. Acta 285 (1996) 309.
[78] H.E. Kissinger, Anal. Chem. 29 (1957) 1702.
[79] T. Akahira, T. Sunose, Res. Report Chiba Inst. Technol. 16 (1971) 22.
[80] A.W. Coats, J.P. Redfern, Nature 201 (1964) 68.
[81] S. Vyazovkin, A.I. Lesnikovich, Thermochim. Acta 165 (1990) 273.
[82] S. Vyazovkin, N. Sbirrazzuoli, Macromol. Rapid Commun. 27 (2006) 1515.
[83] J. Criado, J. Morales, Thermochim. Acta 16 (1976) 382.
[84] A.I. Lesnikovich, S.V. Levchik, J. Therm. Anal. 27 (1983) 89.
[85] A.I. Lesnikovich, S.V. Levchik, J. Therm. Anal. 30 (1985) 237.
[86] L.A. Perez-Maqueda, J.M. Criado, F.J. Gotor, J. Malek, J. Phys. Chem. A 106 (2002) 2862.
[87] J.H. Sharp, G.W. Brindley, B.N. Achar, J. Am. Ceram. Soc. 49 (1966) 379.
[88] F.J. Gotor, J.M. Criado, J. Malek, N. Koga, J. Phys. Chem. A 104 (2000) 10777.
[89] J. Malek, Thermochim. Acta 355 (2000) 239.
[90] J. Malek, Thermochim. Acta 138 (1989) 337.
[91] J.M. Criado, J. Malek, A. Ortega, Thermochim. Acta 147 (1989) 377.
[92] N. Koga, Thermochim. Acta 258 (1995) 145.
[93] J. Malek, J.M. Criado, Thermochim. Acta 236 (1995) 61.
[94] J. Malek, T. Mitsuhashi, J.M. Criado, J. Mater., Res. 16 (2001) 1862.
[95] T. Ozawa, J. Therm. Anal. 2 (1970) 325.
[96] M. Reading, Thermochim. Acta 135 (1988) 37.
[97] J.R. Locatelli, E.C. Rodrigues, A.B. Siqueira, E.Y. Ionashiro, G. Bannach, M. Ionashiro, J. Therm. Anal. Calorim. 90 (2007) 737.
[98] A. Terakita, S.R. Byrn, J. Pharm. Sci. 95 (2006) 1162.
[99] W. Tang, Y. Liu, H. Zhang, C. Wang, Thermochim. Acta 408 (2003) 39.
[100] A. Rotaru, M. Gosa, J. Therm. Anal. Calorim. 97 (2009) 421.
[101] H.L. Friedmann, J. Polym. Sci. C 50 (1965) 183.
[102] W. Tang, D. Chen, Thermochim. Acta 433 (2005) 72.
[103] A. Ortega, Thermochim. Acta 474 (2008) 81.
[104] A. Rotaru, M. Gosa, P. Rotaru, J. Therm. Anal. Calorim. 94 (2008) 367.
[105] D. Kisailus, B. Schwenzer, J. Gomm, J.C. Weaver, D.E. Morse, J. Am. Chem. Soc. 128 (2006) 10276.